Biogeosciences, 17, 567–580, 2020
https://doi.org/10.5194/bg-17-567-2020

Biogeosciences Open Access EGU

Leaf wax *n*-alkane patterns and compound-specific δ^{13}C of plants and topsoils from semi-arid and arid Mongolia

Julian Struck[1], **Marcel Bliedtner**[1,2], **Paul Strobel**[1], **Jens Schumacher**[3], **Enkhtuya Bazarradnaa**[4], **and Roland Zech**[1]

[1]Institute of Geography, Friedrich Schiller University Jena, Löbdergraben 32, 07743 Jena, Germany
[2]Institute of Geography and Oeschger Centre for Climate Change Research, University of Bern, Hallerstrasse 12, 3012 Bern, Switzerland
[3]Institute of Mathematics, Friedrich Schiller University Jena, Ernst-Abbe-Platz 2, 07743 Jena, Germany
[4]Institute of Plant and Agricultural Sciences, Mongolian University of Life Sciences, Darkhan, Mongolia

Correspondence: Julian Struck (julian.struck@uni-jena.de)

Received: 25 June 2019 – Discussion started: 23 July 2019
Revised: 3 January 2020 – Accepted: 10 January 2020 – Published: 5 February 2020

Abstract. Leaf wax *n*-alkane patterns and their compound-specific δ^{13}C signatures are valuable proxies for paleoenvironmental reconstructions. So far, their potential has not been investigated in semi-arid to arid Mongolia. We have therefore analysed the leaf wax *n*-alkanes and their compound-specific δ^{13}C signature of five plant species (*Poaceae*, *Cyperaceae*, *Artemisia* spp., *Caragana* spp. and *Larix* sp.) and topsoils (0–5 cm) along two transects in central and southern Mongolia.

Grasses show a distinct dominance of the *n*-C_{31} homologue, whereas the shrubs *Caragana* spp. and *Artemisia* spp. are dominated by *n*-C_{29}. *Larix* sp. is characterised by the mid-chain *n*-alkanes *n*-C_{23} and *n*-C_{25}. From plant to topsoil, *n*-alkane patterns show the potential to differentiate between grass-covered sites from those covered by *Caragana* spp. *n*-Alkane concentrations and odd-over-even predominance (OEP) of the topsoils are distinctly influenced by mean annual temperature, mean annual precipitation and aridity, likely reflecting the degree of *n*-alkane degradation and biomass production. In contrast, the average chain length (ACL) and the *n*-alkane ratio (n-C_{31}/n-$C_{29} + n$-C_{31}) are not affected by climatic parameters and, thus, are not biased by climate. The compound-specific δ^{13}C signatures are strongly correlated to climate, showing a significant enrichment with increasing aridity, indicating the effect of water use efficiency. Our calibration results suggest that long-chain *n*-alkanes and their compound-specific δ^{13}C signatures have great potential to reconstruct paleoenvironmental and paleoclimatic conditions when used in sediment archives from Mongolia.

1 Introduction

Leaf wax biomarkers such as long-chain *n*-alkanes (n-C_{25} – n-C_{35}) are produced in the plant cuticle as a protection layer against environmental stress and are synthesised by the polyketide biosynthetic pathway, resulting in a distinct odd-over-even predominance (OEP; Eglinton and Hamilton, 1967; Shepherd and Wynne Griffiths, 2006). Due to their water insolubility, chemical inertness and relative resistance against biochemical degradation, leaf wax *n*-alkanes stay well preserved in sediment archives over geological timescales and serve as valuable biomarkers for former environmental conditions (Eglinton and Eglinton, 2008). During the last decades, leaf wax *n*-alkanes have increasingly been used for paleoenvironmental reconstructions in lake sediments (Aichner et al., 2017; Rach et al., 2017; Schwark et al., 2002; Sun et al., 2016), marine sediments (Castañeda et al., 2009; Rommerskirchen et al., 2006; Schefuss et al., 2005), loess–paleosol sequences (Häggi et al., 2019; Schäfer et al., 2018; Zech et al., 2013) and fluvial sediment–paleosol sequences (Bliedtner et al., 2018b).

The relative homologue distribution of leaf wax *n*-alkanes has been used as a chemotaxonomic marker to differentiate among vegetation forms and thus reconstruct paleovegetation: the *n*-alkanes *n*-C_{27} and *n*-C_{29} are thought to be

mainly produced by deciduous trees and shrubs, whereas n-C_{31} and n-C_{33} are mainly produced by grasses and herbs (Bliedtner et al., 2018a; Schäfer et al., 2016; Vogts et al., 2009). The compound-specific δ^{13}C signature of leaf wax n-alkanes has also been used for reconstructing changes in the vegetation composition of C_3 (-20‰ to -35‰) and C_4 (-10‰ to -14‰) plants (Castañeda et al., 2009; Lane, 2017; Rao et al., 2016; Rommerskirchen et al., 2006) and give additional paleoclimatic information about drought stress and arid conditions for C_3 plants (Aichner et al., 2010a, b; Schäfer et al., 2018). Several studies have shown a strong correlation between the δ^{13}C leaf wax signal of C_3 plants and water use efficiency (WUE) that is influenced by precipitation, temperature and evapotranspiration and describes the stomata conductance of a plant to avoid water loss (Diefendorf and Freimuth, 2017; Farquhar et al., 1982; Rao et al., 2017). Along a 400 mm isohyet in China, J. Wang et al. (2018b) have shown that the compound-specific δ^{13}C signature of leaf wax n-alkanes is strongly correlated to temperature, with strongest correlations observed for the average temperature of June, July and August (J. Wang et al., 2018b). Thus, warmer and dryer conditions cause an increase in WUE, resulting in an ^{13}C enrichment and cooler and wetter conditions vice versa (Aichner et al., 2015; Castañeda et al., 2009; Diefendorf and Freimuth, 2017; J. Wang et al., 2018b).

Although leaf wax n-alkane patterns and compound-specific δ^{13}C have been increasingly used in sediment archives for paleoenvironmental reconstructions within the last decades, they need to be calibrated regionally on recent reference material before any paleoenvironmental reconstruction can be made. The need for regional calibrations has been emphasised by the fact that Bush and McInerney (2013) questioned whether leaf wax n-alkane patterns can discriminate between modern vegetation forms on a global scale, while several regional studies found them discriminating on a regional scale. Although the most abundant homologues differ from region to region, a good discrimination power has been reported from Europe (Schäfer et al., 2016; Zech et al., 2009, 2010), the Caucasus region (Bliedtner et al., 2018a), North and South America (Diefendorf et al., 2015; Feakins et al., 2016; Lane, 2017), and the African rainforest and savanna (Vogts et al., 2009).

However, when interpreting leaf wax n-alkanes and their compound-specific δ^{13}C signature several potential pitfalls, such as species-specific and intra-leaf variations (Diefendorf et al., 2011; Gao et al., 2015), the influence of environmental and climatic factors (Carr et al., 2014; Diefendorf and Freimuth, 2017; Farquhar et al., 1982; Hoffmann et al., 2013; Rao et al., 2017; Tipple et al., 2013), the dependency on altitude (Feakins et al., 2018; Hultine and Marshall, 2000), and n-alkane degradation (Brittingham et al., 2017; Buggle et al., 2010; Li et al., 2018a), have to be considered and accounted for. So far, such regional calibration studies on recent leaf wax n-alkane patterns, compound-specific δ^{13}C and potential climatic biases on the leaf wax signal do not exist for Mongolia.

Thus, this study investigates leaf wax n-alkane patterns and compound-specific δ^{13}C of modern plants and topsoils from semi-arid and arid Mongolia to evaluate their potential for regional paleovegetation and paleoclimate reconstructions. More specifically, we tested the chemotaxonomic potential of leaf wax n-alkane patterns from five dominant plant species and whether their homologue distribution can be used to discriminate between woody shrubs and grasses–herbs on a regional scale. Moreover, we investigate differences in the compound-specific δ^{13}C signature of leaf wax from plants and topsoils and how the plant signal is incorporated into the topsoil. Since only the topsoils represent an averaged decadal leaf wax signal, we check for potential environmental and climatic influences by correlating the leaf wax n-alkane patterns and δ^{13}C with altitude, mean annual temperature (MAT), mean annual precipitation (MAP) and the aridity index (AI). While we test that the n-alkane patterns are not biased by climatic influences, we test the potential of leaf wax δ^{13}C to reflect on MAT, MAP and aridity. Additionally, we test for a potential bias from altitude on leaf wax n-alkane patterns and the δ^{13}C signal. Therefore, our calibration results will be a base for future robust paleovegetational and paleoclimate reconstructions in semi-arid and arid Mongolia using leaf wax n-alkanes from regional sediment archives. Such lacustrine, loess–paleosol and colluvial sediment archives have been increasingly investigated in semi-arid and arid Mongolia and could potentially be used for future paleoenvironmental reconstructions based on leaf wax n-alkanes (Klinge et al., 2017; Peck et al., 2002; Prokopenko et al., 2007; Rudaya and Li, 2013; Wang et al., 2011).

2 Material and methods

2.1 Geographical setting and sampling

Semi-arid and arid Mongolia is a highly continental region characterised by harsh and long winters and hot and short summers (Dashkhuu et al., 2015). Mongolia is located at the interface of three major atmospheric circulation systems controlling the regional climate (Fig. 1). The summer climate is dominated by the East Asian summer monsoon (EASM) and the Westerlies, which provide most of the yearly moisture and precipitation during the summer months; i.e. 75 % of the annual precipitation falls in June, July and August (Rao et al., 2015; Wang and Feng, 2013). The dry and cold winter climate is dominated by the Siberian high, which mostly blocks the moisture supply from the Westerlies during winter (Peck et al., 2002). The Mongolian climate has a north–south gradient in MAT and MAP, with increasing MAT from north to south and MAP vice versa (Fig. 2a, b; Harris et al., 2014). This north–south gradient in temperature and precipitation is further reflected by the AI (Fig. 2c) and in the distribution of

regional vegetation biomes with taiga and mountain and forest steppe in northern and central Mongolia and steppe and desert steppe in southern Mongolia (Hilbig, 1995; Klinge and Sauer, 2019).

Topsoils (0–5 cm) were sampled along a north–south transect (transect I; see Fig. 1 for location) in June 2016, and plants and topsoils (0–5 cm) were sampled along an east–west transect (transect II; see Fig. 1 for location) in July–August 2017. Along transect II, the topsoils were sampled together with the dominant plant species (5 m^2 around the topsoil sampling site), which comprise the woody shrub *Caragana* spp.; the grasses and herbs *Poaceae*, *Cyperaceae* and *Artemisia* spp.; and *Larix* sp. as a coniferous tree. *Artemisia* spp. summarises different herbaceous species and perennial "shrubby" species with a woody base (e.g. *Artemisia frigida*). Transect I covers an altitudinal range between 1224 and 1611 m a.s.l., and MAT and MAP range from −1.7 to 5.5 °C and 99 to 276 mm a^{-1}. Transect II covers an altitudinal range between 1333 and 2792 m a.s.l. and a range from −7.3 to −0.5 °C and 210.8 to 276.2 mm a^{-1} in MAT and MAP, respectively, and is separated into the Ögiinuur catchment (TS II-A), an altitudinal transect (TS II-B) and the Telmen Nuur catchment (TS II-C; Fig. 2; Fick and Hijmans, 2017).

2.2 Leaf wax analysis

2.2.1 Leaf wax extraction and quantification

Total lipids of the topsoils (∼ 35 g) from transect I were extracted at the University of Bern, Switzerland, using accelerated solvent extraction (Dionex ASE 200: 6.9 MPa, 100 °C) with 60 mL dichloromethane : methanol (DCM : MeOH; 9 : 1, v/v) over three extraction cycles as described by Bliedtner et al. (2018b). The total lipids of topsoils (∼ 10 g) and plant leaves (∼ 1 g) from transect II were extracted at the Friedrich Schiller University of Jena, Germany, using ultrasonic extraction with 20 mL DCM : MeOH (9 : 1, v/v) over three cycles as described by Bliedtner et al. (2018a).

The total lipid extract from both transects was separated over aminopropyl pipette columns (Supelco; 45 µm) into (i) an apolar fraction including the n-alkanes, (ii) a more polar fraction and (iii) an acid fraction. n-Alkanes were eluted with ∼ 4 mL hexane and additionally cleaned over coupled silver–nitrate ($AgNO_3$) and zeolite pipette columns. n-Alkanes were subsequently dissolved in hydrofluoric acid and liquid–liquid recovered with hexane. Identification and quantification of the n-alkanes was performed on an Agilent 7890B gas chromatograph equipped with an Agilent HP5MS column (30 m × 320 µm × 0.25 µm film thickness) and a gas chromatography–flame ionisation detector (GC–FID). For identification and quantification, external n-alkane standards with a known concentration (n-alkane mix: n-C_{21} − n-C_{40}; Supelco) were run with each sequence.

2.2.2 Compound-specific δ^{13}C analysis

Compound-specific carbon isotopes were measured for the most abundant n-alkanes, n-C_{29} and n-C_{31}. Isotope measurements were performed on an isoprime visION isotope ratio mass spectrometer coupled to a gas chromatograph (Agilent 7890B GC) equipped with an Agilent HP5GC column (30 m × 320 µm × 0.25 µm film thickness) via a GC5 pyrolysis–combustion interface. The GC5 operated in the combustion mode, with a CuO reactor at 850 °C. Samples were injected in splitless mode and measured in triplicates. n-Alkane standards (n-C_{27}, n-C_{29} and n-C_{33}) with known isotopic composition (Schimmelmann standard, Indiana) were measured as duplicates after every third triplicate. The standard deviation for the triplicate measurements was < 0.7‰, and the standard deviation for the standards was < 0.2‰ ($n = 102$). Carbon isotopic composition is given in the delta notation (δ^{13}C) versus the Vienna Pee Dee Belemnite standard (VPDB).

2.2.3 Data analysis

n-Alkane concentrations ($\sum$ n-Alkane) are given in micrograms per gram (µg g^{-1}) dry weight and were calculated as the sum of n-C_{25} to n-C_{35}. Additionally, we tested the n-alkane concentrations as the sum of n-C_{23} to n-C_{35} because of the high proportions of n-C_{23} in *Larix* sp. However, differences between both n-alkane concentrations are minor, and, thus, we present the n-alkane concentrations including n-C_{23} in the Supplement. The OEP was calculated according to Hoefs et al. (2002) and serves as a proxy for degradation, with values below 5 indicating enhanced n-alkane degradation (Buggle et al., 2010; Zech et al., 2009, 2010):

$$\mathrm{OEP} = \frac{n\text{-}C_{27} + n\text{-}C_{29} + n\text{-}C_{31} + n\text{-}C_{33}}{n\text{-}C_{26} + n\text{-}C_{28} + n\text{-}C_{30} + n\text{-}C_{32}}. \quad (1)$$

The average chain length (ACL) was determined after Poynter et al. (1989) and is used to distinguish between leaf wax predominantly produced by deciduous trees and shrubs (n-C_{27} and n-C_{29}) and grasses and herbs (n-C_{31} and n-C_{33}; Bliedtner et al., 2018a):

$$\mathrm{ACL} = \frac{27 \cdot n\text{-}C_{27} + 29 \cdot n\text{-}C_{29} + 31 \cdot n\text{-}C_{31} + 33 \cdot n\text{-}C_{33}}{n\text{-}C_{27} + n\text{-}C_{29} + n\text{-}C_{31} + n\text{-}C_{33}}. \quad (2)$$

A normalised n-alkane ratio was calculated for the most abundant n-alkanes, n-C_{29} and n-C_{31}:

$$n\text{-Alkane ratio} = \frac{n\text{-}C_{31}}{(n\text{-}C_{29} + n\text{-}C_{31})}. \quad (3)$$

2.3 Statistical analysis

Differences in n-alkane concentration, OEP, ACL, n-alkane ratio and compound-specific δ^{13}C among plant species and

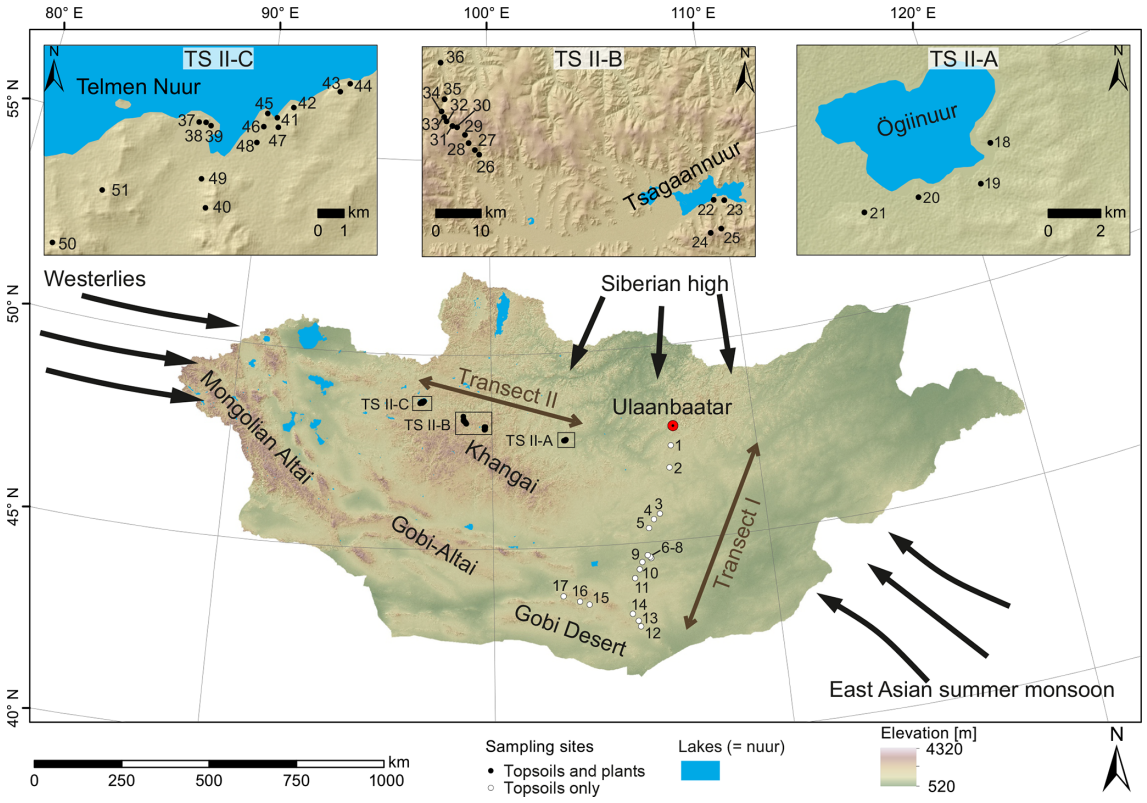

Figure 1. Map of Mongolia (SRTM digital elevation model). The black and white circles mark the sampling sites along transect I and II. Black arrows indicate the influence of three major atmospheric circulation systems: the Westerlies, the East Asian summer monsoon and the Siberian high. Submaps show (TS II-A) the Ögiinuur catchment, (TS II-B) an altitude transect near the Tsagaannuur catchment and (TS II-C) the Telmen Nuur catchment in more detail.

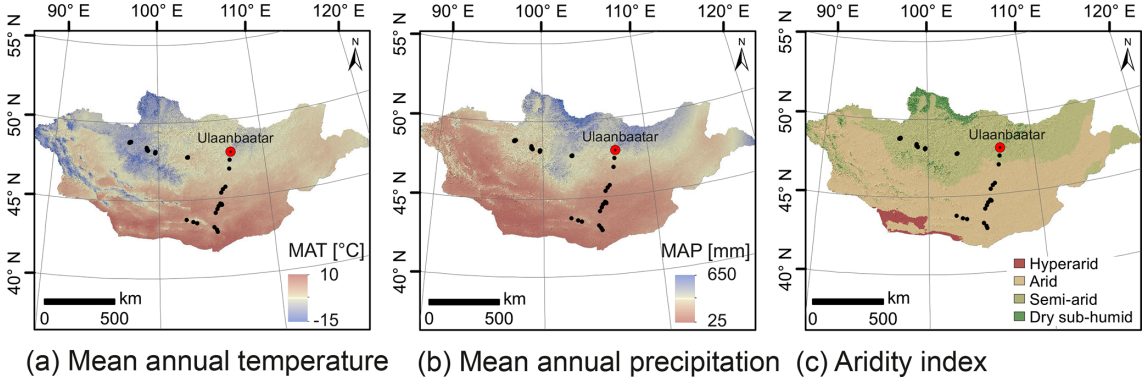

Figure 2. Climate and environmental conditions of Mongolia. Mean annual temperature **(a)**, mean annual precipitation **(b)** and the aridity index **(c)**. MAT and MAP are based on the WorldClim dataset of Fick and Hijmans (2017); the AI is based on the Global Aridity Index and Potential Evapotranspiration Climate Database v2 of Trabucco and Zomer (2019).

between topsoils and plants were analysed using analysis of variance (ANOVA) followed by pairwise comparisons based on Tukey's honestly significant difference. Since the relative homologue distribution of the n-alkanes is important for the discrimination between plant species, the n-alkane patterns were analysed as compositional data according to Aitchison (2003). Correlations of n-alkane concentration, OEP, ACL, n-alkane ratio and compound-specific δ^{13}C with climatic parameters and altitude were tested using weighted linear or polynomial regression. The environmental parameters MAT and MAP were derived from the WorldClim 2.0 dataset (1970–2000; 30 s resolution; Fick and Hijmans, 2017) and the AI from the Global Aridity Index and Potential Evapotranspiration (ET0) Climate Database v2 (1970–2000; 30 s

resolution; Trabucco and Zomer, 2019). The altitude was extracted from the Shuttle Radar Topography Mission (SRTM) data (Jarvis et al., 2008). Regressions were tested only for the topsoils because they represent an averaged leaf wax signal over some decades (Angst et al., 2016) and can thus be correlated with the WorldClim and the Global Aridity Index data that represent averaged climate data over 30 years. In contrast, plants only reflect an annual signal of the sampling year 2017 and cannot be correlated with the available climatic parameters from the WorldClim and the Global Aridity Index dataset, and also annual climate data for the sampling year 2017 are not available. Model selection was based on hierarchical comparison of models with increasing polynomial order using F ratios. Goodness of fit of the final models was assessed using weighted R^2 values. All statistical analyses were done using the statistical software system R (R Core Team, 2019) and the package compositions (Boogaart, 2013) for compositional data analysis.

3 Results

3.1 n-Alkane patterns in plants and topsoils

Leaf wax n-alkanes are present in all analysed plants and topsoils and show a distinct OEP (Fig. 3). For the analysed plants from transect II, the most abundant n-alkane homologues vary among the plant species: *Poaceae* and *Cyperaceae* tend to be dominated by n-C_{31}, and *Artemisia* spp. and *Caragana* spp. tend to be dominated by n-C_{29}. *Larix* sp. is dominated by the mid-chain n-alkane n-C_{25}. The topsoils from both transects are mostly dominated by n-C_{31} (Fig. 3). Figure 4 illustrates differences in n-alkane concentrations, OEP, ACL and the n-alkane ratio of the analysed plant species and topsoils, and Table 1 shows the corresponding level of significance. n-Alkane concentrations are significantly higher in plants than topsoils ($p = 5.1e^{-07}$). Plants range from 9 to 2508 $\mu g\, g^{-1}$, with *Caragana* spp. having significantly the highest concentrations and *Larix* sp. having the lowest concentrations (Fig. 4a; Table 1). n-Alkane concentrations in topsoils range from 0.2 to 59 $\mu g\, g^{-1}$, with transect I having much lower concentrations than transect II (Fig. 4a). Plants show a wide-ranging OEP, with values ranging between 4 and 39. The highest OEP values are observed for *Caragana* spp., followed by *Poaceae*, *Cyperaceae*, and *Artemisia* spp. and *Larix* sp. Topsoils have generally lower OEP values than plants, ranging from 1.5 up to 5.5 for transect I and from 4.8 to 19 for transect II (Fig. 4b). ACL values of plants range from 28.3 to 30.8, with *Larix* sp. showing significantly lower ACLs compared to the other plants (Table 1). ACL values for topsoils are higher but in the same range as most plant species, ranging from 29.6 to 30.4 along transect I and from 29.2 to 31.8 along transect II (Fig. 4c). The n-alkane ratio shows values between 0.16 and 0.8. *Poaceae* and *Cyperaceae* tend to have the highest values, and *Caragana* spp. and *Larix* sp. tend to have the lowest values. The topsoils range from 0.42 to 0.75 for both transects (Fig. 4d).

3.2 Compound-specific δ^{13}C

Compound-specific δ^{13}C values were measured for the most abundant n-alkanes, n-C_{29} and n-C_{31} (Fig. 5). Plants show δ^{13}C values between -36‰ and -29.5‰ for n-C_{29} and between -35.8‰ and -30.3‰ for n-C_{31}, with *Larix* sp. being the most enriched in leaf wax ^{13}C among all plant species. In comparison to plants, topsoils tend to be more enriched in ^{13}C, with a larger scatter, and range from -33.8‰ to -25.6‰ for n-C_{29} and from -34.3‰ to -25.2‰ for n-C_{31}, with a distinct enrichment along transect I (Fig. 5). Compound-specific δ^{13}C values of n-C_{29} and n-C_{31} differ significantly between topsoils from transect I and transect II but not significantly between plant species and between plant species and topsoils from transect II (Table 1).

4 Discussion

4.1 n-Alkane patterns in plants

The plant species from Mongolia show distinct differences in their relative n-alkane homologue pattern (Fig. 3). The grasses *Poaceae* and *Cyperaceae* are dominated by n-C_{31}, whereas the woody shrub *Caragana* spp. is dominated by n-C_{29}. These findings are in line with previous regional studies from the Tibetan Plateau (Cheung et al., 2015; Z. Wang et al., 2018), the Chinese Loess Plateau (Liu et al., 2018) and the Caucasus region (Bliedtner et al., 2018a), which report n-C_{31} being mainly produced by grasses and herbs and n-C_{29} by deciduous trees and shrubs. Although *Artemisia* spp. could be expected to be herbaceous, with a dominance in n-C_{31}, our results show a distribution maximum at n-C_{29}; i.e. it is more similar to the woody shrub *Caragana* spp. than to the grass species. This is not necessarily contradictory and corroborates the findings of J. Wang et al. (2018b) along a 400 mm isohyet transect from north-western to central China, which reports that *Artemisia* can grow both as herbaceous plant and as a woody shrub (e.g. *Artemisia frigida*). In contrast to the other plant species, the coniferous tree *Larix* sp. is dominated by the mid-chain n-alkanes n-C_{23} and n-C_{25}, resulting in a significantly lower ACL (Fig. 4c; Table 1). However, statistically significant differences between the ACLs of the other plant species are not evident, although the relative homologue pattern reveals differences among them (Table 1; Figs. 3 and 4c). The ACLs of the grasses and herbs *Poaceae* and *Cyperaceae* and *Artemisia* spp. and the woody shrub *Caragana* spp. have only slight differences and a small range, between 29.6 and 29.9. This is due to a strong ACL scattering of the grasses and herbs that overlap the ACL of the woody shrubs (Fig. 4c). Thus, a clear chemotaxonomic discrimination between grasses and herbs and woody shrubs is not given by the ACL for the investigated modern plants from

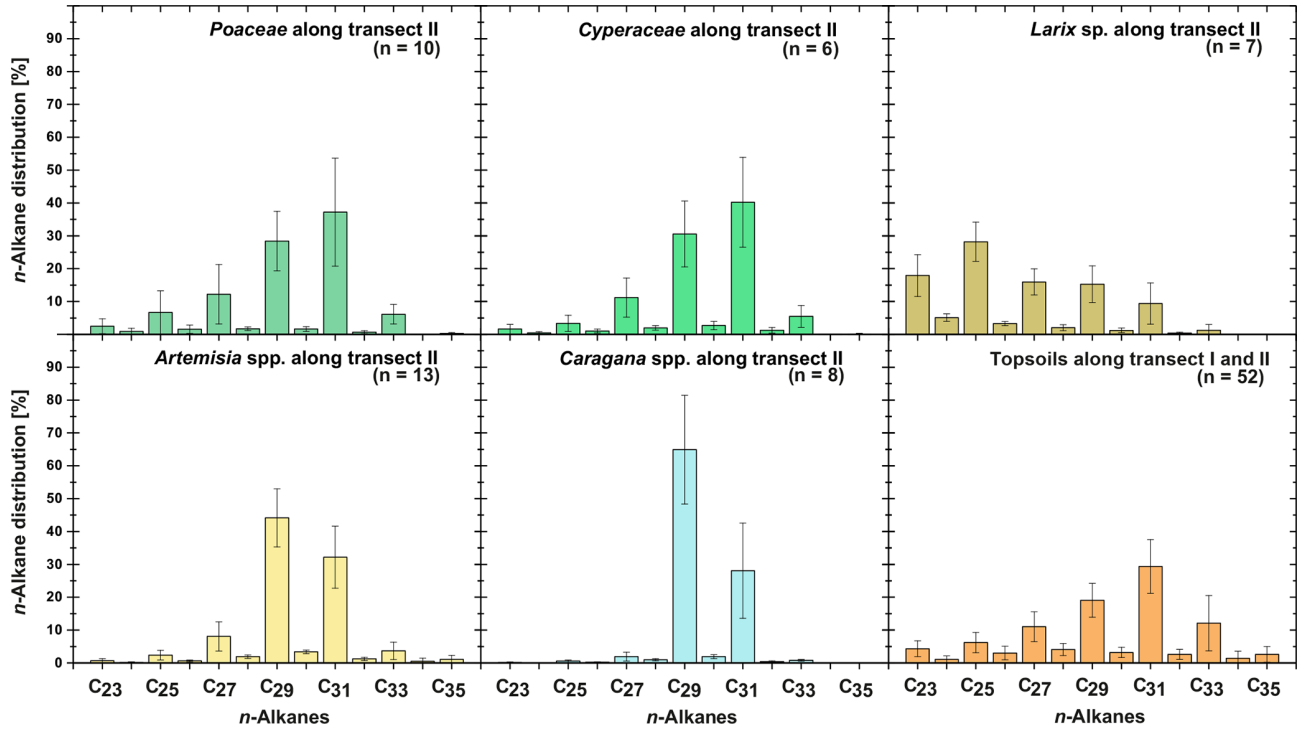

Figure 3. n-Alkane patterns of plants (transect II) and topsoils (transect I and II) from Mongolia. The bars show the mean values ±SD.

Table 1. ANOVA p values, indicating differences among plant species and between topsoils and plants for n-alkane pattern and compound-specific δ^{13}C (n-C_{29} and n-C_{31}). Bold values indicate significance ($\alpha = 0.05$). TS is topsoil.

	$\sum n$-Alkane (n-C_{25} – n-C_{35})	OEP	ACL	n-Alkane ratio	$\delta^{13}C_{29}$	$\delta^{13}C_{31}$
Poaceae–*Cyperaceae*	1.000	0.979	1.000	0.999	1.000	0.999
Larix sp.–*Cyperaceae*	0.505	**0.032**	**0.000**	**0.010**	0.203	0.315
Poaceae–*Artemisia* spp.	0.999	0.392	0.986	0.069	0.998	1.000
Poaceae–*Caragana* spp.	**0.000**	**0.000**	0.861	**0.000**	0.814	0.995
Poaceae–*Larix* sp.	0.325	**0.001**	**0.000**	**0.007**	0.164	0.381
Cyperaceae–*Artemisia* spp.	0.999	0.948	0.959	0.079	0.995	0.991
Cyperaceae–*Caragana* spp.	**0.000**	**0.000**	0.802	**0.000**	0.812	0.965
Caragana spp.–*Artemisia* spp.	**0.000**	**0.000**	0.991	0.185	0.928	0.999
Larix sp.–*Artemisia* spp.	0.137	0.083	**0.000**	0.806	0.230	0.425
Larix sp.–*Caragana* spp.	**0.000**	**0.000**	**0.004**	0.946	1.826	0.734
TS Transect II–*Poaceae*	0.063	**0.000**	0.204	0.801	0.085	0.198
TS Transect II–*Cyperaceae*	0.259	0.075	0.658	0.99	0.162	0.219
TS Transect II–*Artemisia* spp.	**0.006**	0.251	**0.012**	**0.000**	0.132	0.181
TS Transect II–*Caragana* spp.	**0.000**	**0.000**	**0.009**	**0.000**	0.994	0.799
TS Transect II–*Larix* sp.	1.000	0.573	**0.000**	**0.000**	0.818	0.996
TS Transect I–TS Transect II	**0.003**	**0.000**	0.082	0.273	**0.000**	**0.006**

Mongolia. A better chemotaxonomic discrimination is provided by the n-alkane ratio n-C_{31} / (n-C_{29} + n-C_{31}), which is based on the most abundant homologues, n-C_{29} and n-C_{31}. The n-alkane ratio significantly separates the grasses *Poaceae* and *Cyperaceae* from the woody shrub *Caragana* spp. and the coniferous tree *Larix* sp. (Fig. 4d). The n-alkane ratio of *Artemisia* spp. lies in between the woody shrubs and grasses, most likely because of their ability to grow as both herbaceous and woody shrubs (Fig. 4d). This is further expressed statistically, as the n-alkane ratio of *Artemisia* spp. is equal to that calculated from both *Caragana* spp. and the grass species (Table 1). Besides *Artemisia* spp., the n-alkane

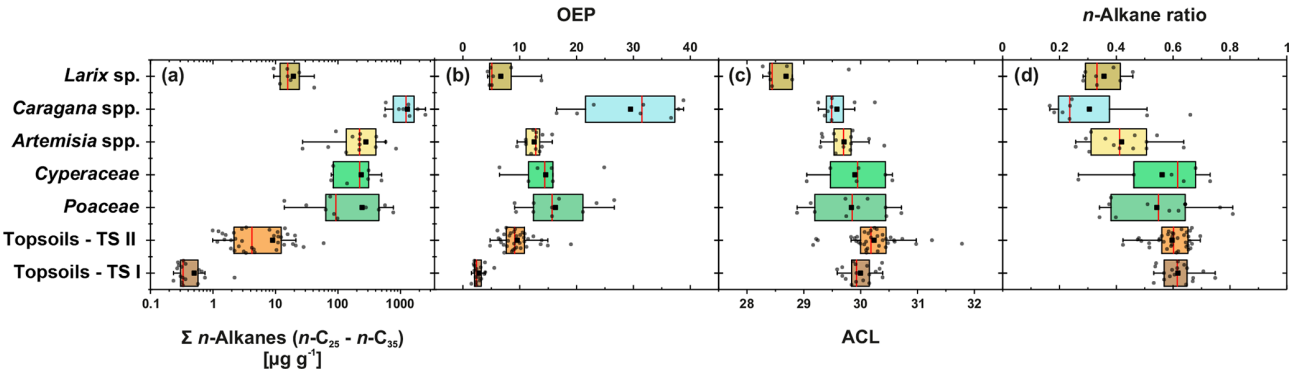

Figure 4. n-Alkane concentration (n-C_{25} − n-C_{35}) **(a)**, OEP **(b)**, ACL **(c)** and n-alkane ratio (n-C_{31} / (n-C_{29} + n-C_{31})) **(d)** of plants and topsoils from Mongolia (n: *Larix* sp. = 7, *Cyperaceae* = 6, *Poaceae* = 10, *Caragana* spp. = 8, *Artemisia* spp. = 13, topsoils TS I = 17, topsoils TS II = 35). The boxplots indicate median values (red lines), mean values (black squares), interquartile ranges with lower (25 %) and upper (75 %) quartiles (box), outlier (whiskers), and investigated samples (grey circles). See Table 1 for statistics.

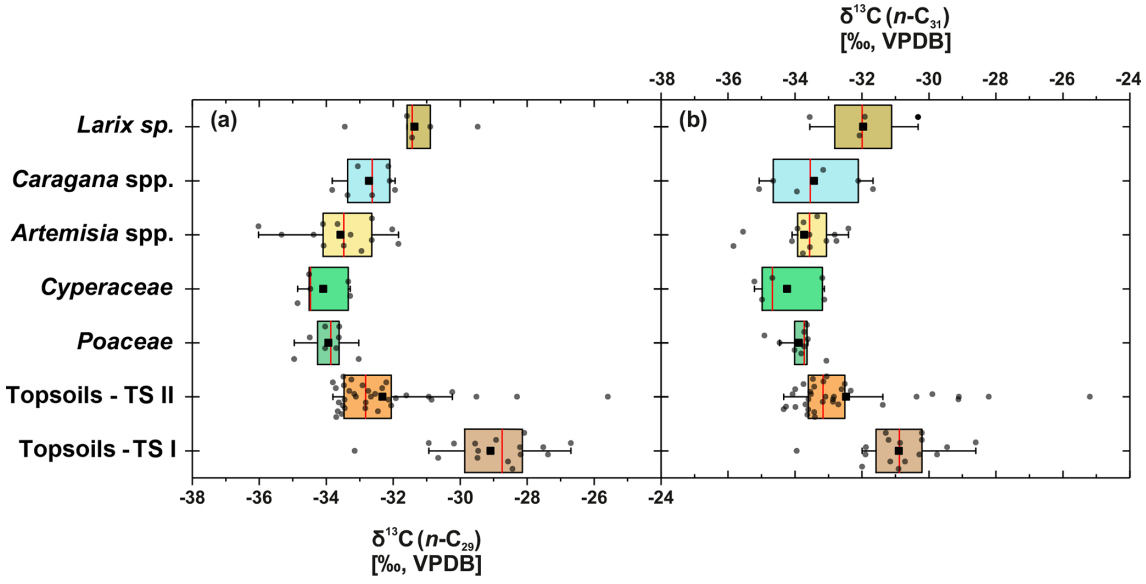

Figure 5. Compound-specific δ^{13}C of plants and topsoils from Mongolia. **(a)** Compound-specific $\delta^{13}C_{29}$ (n: *Larix* sp. = 5, *Cyperaceae* = 5, *Poaceae* = 8, *Caragana* spp. = 7, *Artemisia* spp. = 13, topsoils TS I = 16, topsoils TS II = 34). **(b)** $\delta^{13}C_{31}$ (n: *Larix* sp. = 4, *Cyperaceae* = 5, *Poaceae* = 9, *Caragana* spp. = 6, *Artemisia* sp. = 13, topsoils TS I = 16, topsoils TS II = 34). The boxplots indicate median values (red lines), mean values (black squares), interquartile ranges with lower (25 %) and upper (75 %) quartiles (box), outlier (whiskers), and investigated samples (grey circles). See Table 1 for statistics.

ratio has the chemotaxonomic potential to discriminate significantly between *Larix* sp. and grasses as well as between *Caragana* spp. and grasses. However, the n-alkane patterns from *Larix* sp. with their mid-chain dominance have to be interpreted with caution when comparing species-specific differences to the long-chain dominated plant species, which is mostly due to the fact that *Larix* sp. only produce small amounts of n-alkanes. When incorporated into the soil, the coniferous n-alkane signal from *Larix* sp. should become overproportionately overprinted by the undergrowth of the grasses and herbs (Diefendorf et al., 2011; Schäfer et al., 2016).

4.2 Compound-specific δ^{13}C of plants

The compound-specific δ^{13}C values of the n-alkanes from our investigated plants from transect II show consistent δ^{13}C values among the plant species, except for *Larix* sp., and are in a typical range of C_3 plants (Fig. 5; Tipple and Pagani, 2007). Although Pyankov et al. (2000) have reported C_4 plants in Mongolia among 16 plant families, including *Poaceae*, which are not evident along our sampled plant transect. While some C_4 plants have been found in the Khangai Mountains, their distribution is mainly limited to the semi-arid steppe and semi-desert areas in southern Mongo-

lia and the Gobi desert, i.e. beyond our plant sampling sites (Pyankov et al., 2000; Su et al., 2011). Statistically significant differences did not exist between the most abundant homologues, n-C_{29} and n-C_{31} ($p = 1$), indicating that no different fractionation occurred during biosynthesis (J. Wang et al., 2018b). Consistent δ^{13}C values between the most abundant homologues are in good agreement with compound-specific δ^{13}C analyses of three *Artemisia* species (*Artemisia argyi*, *Artemisia capillaris* and *Artemisia scoparia*) along a 400 mm isohyet in China (J. Wang et al., 2018b). While no differences are found between the δ^{13}C values of the grasses and herbs and woody shrubs, only *Larix* sp. is enriched up to 2‰, but this is still in the range of C_3 plants (Fig. 5; Table 1). Such an enrichment of coniferous trees compared to other plants might be explained by differences in species-specific fractionation (Diefendorf et al., 2015).

4.3 Comparing n-alkane patterns and compound-specific δ^{13}C of plants versus topsoils

4.3.1 The leaf wax signal from plants to topsoils along transect II

Along transect II, modern plants have higher n-alkane concentration than the topsoils, with *Artemisia* spp. and *Caragana* spp. having significantly higher n-alkane concentrations than the respective topsoils (Fig. 4a; Table 1). Thus, lower n-alkane concentration in the topsoils indicates that n-alkanes become diluted during the incorporation from plant biomass into the topsoil (Fig. 4a). Likewise, the OEP decreases from plants to topsoil and indicates enhanced organic matter degradation (Buggle et al., 2010; Schäfer et al., 2016) and microbial alteration (Fig. 4b; Schulz et al., 2012). Despite possible degradation effects during soil development, the topsoils show distinct OEP values between 4.8 and 19, still indicating good preservation (Zech et al., 2009). Along transect II, one exception in terms of the higher n-alkane concentration and OEP is TSC10 Ah1, showing 59 µg g^{-1} and 19, respectively (Fig. 1; sampling site 25). Site TSC10 is characterised by stagnating soil conditions with a distinct organic rich topsoil, limiting organic matter degradation and microbial alteration of n-alkanes (Hoefs et al., 2002). Thus, TSC10 Ah1 remains exceptional and not comparable to the other topsoils from transects II. Overall, decreasing concentrations and OEP values from plants to topsoils are in good agreement with other regional studies (Bliedtner et al., 2018a; Howard et al., 2018; Li et al., 2018b; Schäfer et al., 2016; Zech et al., 2009).

For the topsoils, n-C_{31} is on average the most abundant n-alkane homologue, indicating a typical n-alkane pattern produced by grasses (Fig. 3; Bliedtner et al., 2018a). The only exceptions are sites covered with *Caragana* spp. ($n = 8$), where higher amounts of n-C_{29} are evident within the respective topsoils and the two *Caragana*-covered topsoils TLC4 Ah1 and TLC6 Ah1 (Fig. 1; sampling sites 40 and 42) even show a dominance of n-C_{29} (Supplement). Thus, the dominant n-C_{29} signal produced by the woody shrubs is also reflected in the respective topsoils. This is further expressed by lower ACLs and n-alkane ratios for those topsoils, which explains the scattering towards n-C_{29} in ACL and 0.4 for the n-alkane ratio, respectively (Fig. 4c, d). At sites covered with *Larix* sp., the mid-chain-length dominance of *Larix* sp. is not reflected in the respective topsoils, which are mainly dominated by n-C_{31} n-alkanes. Thus, n-alkanes from *Larix* sp. must become strongly diluted from plant to topsoil, and the topsoils reflect mostly the n-alkanes from the grassy undergrowth, as previously shown by Schäfer et al. (2016) for several coniferous sites, including *Larix*, *Picea*, *Abies* and *Pinus*. Compared to the plants, the isotopic signature of the topsoils is slightly more enriched but reveal no statistical significance (Fig. 5; Table 1), which is in line with previous studies and might reflect an enrichment by diagenesis from litter to topsoil or a change in vegetation composition (Wu et al., 2019, and references therein).

Environmental information of the plants' compound-specific δ^{13}C signal only reflects one vegetation period, whereas the topsoils' compound-specific δ^{13}C signal reflects environmental variability on decadal timescales, which might explain the ^{13}C-enriched leaf wax n-alkanes in topsoils. However, one topsoil (TLC4 Ah1) shows a strong ^{13}C enrichment of up to ~ -25‰. Such an enrichment might be explained by n-alkane contributions from succulent plants, which tend to be more enriched in ^{13}C within the range of C_3 plants (Boom et al., 2014). Succulents were growing on stone-rich, thin topsoils in the catchment of Telmen Nuur (Fig. 1; TS II-C). For comparison, we sampled the succulent *Orostachys malacophylla* from the Telmen catchment and analysed its compound-specific δ^{13}C isotopes, which yield -24.7‰ for n-C_{29} ($n = 1$) and -25.03‰ for n-C_{31} ($n = 1$). Thus, increased inputs of succulent δ^{13}C might best explain the enriched isotopes in the Telmen catchment and the extreme value of ~ -25‰ from site TLC4.

4.3.2 The leaf wax signal of the topsoils along both transects

The topsoils of both Mongolian transects show distinct differences in n-alkane concentration and OEP, which are higher along transect II and decrease along transect I. This is mostly due to the fact that n-alkane production and degradation are influenced by the climatic gradient along transect I (see Sect. 4.4 and Fig. 2 for more detailed discussion). Besides some n-C_{29} dominated sites with *Caragana* spp., the ACL and the n-alkane ratio show the dominance of n-C_{31}, which indicates the n-alkane origin from the grasses *Poaceae* and *Cyperaceae* (Fig. 4; Bliedtner et al., 2018a; Schäfer et al., 2016; Vogts et al., 2009; Zech et al., 2010). This is further expressed by the results of ANOVA because the ACL and n-alkane ratios from topsoils and grasses are not statistically different (Table 1).

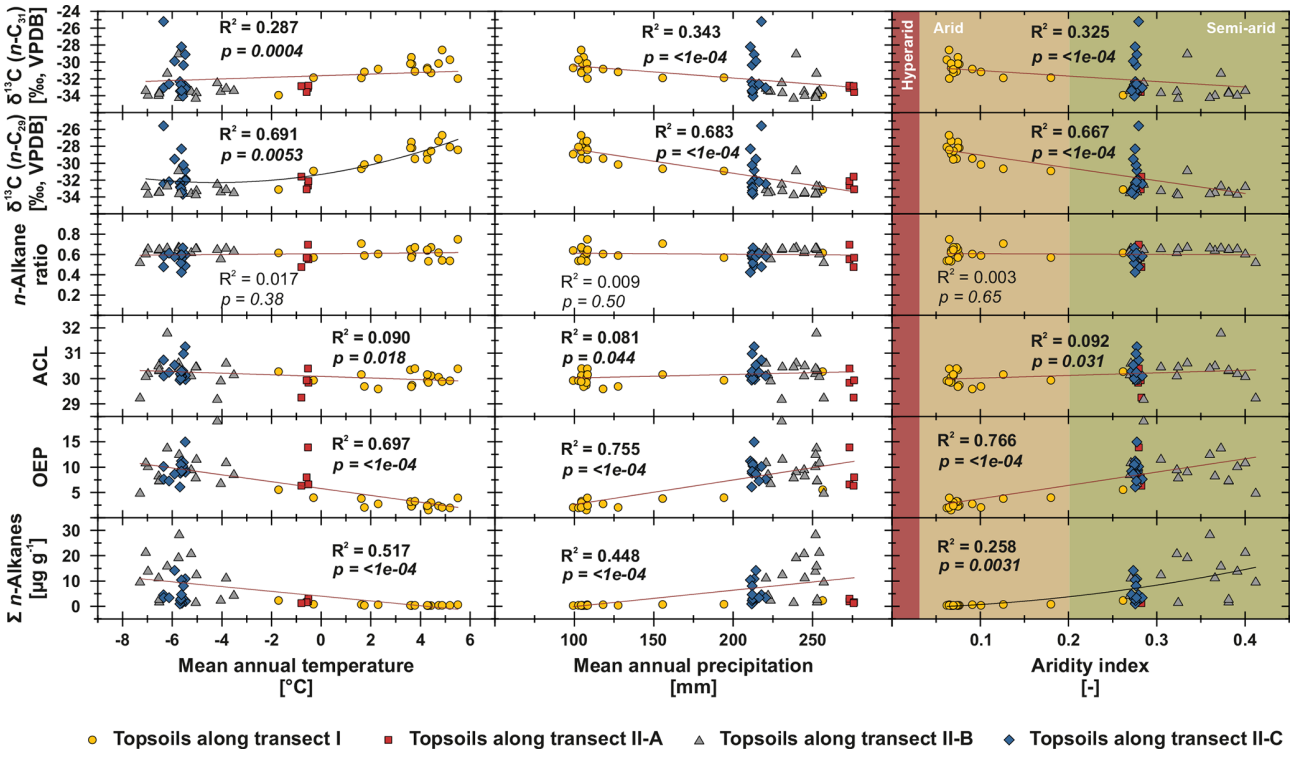

Figure 6. n-Alkane concentration (n-C_{25} – n-C_{35}), OEP, ACL, n-alkane ratio (n-C_{31} / (n-C_{29} + n-C_{31})) and compound-specific δ^{13}C (n-C_{29} and n-C_{31}) from Mongolian topsoils plotted against climatic parameters (MAP, MAT and AI; Fick and Hijmans, 2017; Trabucco and Zomer, 2019). Red trend lines illustrate linear regressions, and black lines illustrate polynomial regressions. Bold values indicate significance ($\alpha = 0.05$).

4.4 Climatic influences on topsoil n-alkane patterns and compound-specific δ^{13}C

To test potential climatic influences on our n-alkane proxies, we correlate them with MAT, MAP and AI (Fig. 6). The n-alkane patterns show that n-alkane concentrations in topsoils and their preservation (OEP) are correlated not only to climatic parameters but also to altitude, indicating higher n-alkane concentrations and better n-alkane preservation above 2000 m a.s.l. (Fig. 7; transect II-B). Since altitude generally controls MAT ($R^2 = 0.624$) and MAP ($R^2 = 0.395$), we suggest that variations along the investigated transects are primarily climate induced. Thus, we detected MAT ($R^2 = 0.517$, $p =< 1e-04$) as the main climatic control parameter on n-alkane concentrations for the topsoils from both transects. Correlations of n-alkane concentration with MAP ($R^2 = 0.448$, $p =< 1e-04$) and AI ($R^2 = 0.258$, $p = 0.0031$) are likewise significant, indicating a clear correlation (Fig. 6). We conclude that lower n-alkane concentrations probably indicate reduced biomass production and enhanced n-alkane degradation in the topsoils. The former even intensifies when combined with livestock grazing (Kölbl et al., 2011, and references therein), especially along transect I (sampling sites 1–17), where biomass production is reduced and overgrazing occurs extensively (Fig. 6). In contrast, sites along transect II-B (above 2000 m a.s.l.) describe a favourable area for plant growth and thus an increase in n-alkane concentrations and OEP (Fig. 7). However, especially transect II-B and II-C are characterised by a distinct scatter, which is mainly the result of variations in plant physiology and site-specific and micro-climatic characteristics which are not covered by the reanalysis data.

Previous studies have shown correlations between the production of the most abundant homologues with climatic parameters and altitude; i.e. common vegetation proxies such as the ACL and n-alkane ratio could reflect changes in MAT, since plants tend to produce longer n-alkanes as a protection against water loss (Bush and McInerney, 2013; Feakins et al., 2016; Sachse et al., 2006; Tipple et al., 2013; J. Wang et al., 2018b, a). However, this could not be observed by the n-alkanes from Mongolian topsoils, since the ACL and the n-alkane ratio as common vegetation proxies show no correlations with MAT, MAP, AI or altitude (Figs. 6, 7).

In contrast, compound-specific δ^{13}C values of the topsoils correlate significantly with climatic parameters. Our results show an enrichment in ^{13}C with increasing temperature, aridity and decreasing precipitation (Fig. 6). This climate-induced enrichment in ^{13}C follows mainly the north–south gradient in decreasing MAP and increasing MAT along transect I from central Mongolia into the Gobi Desert. The

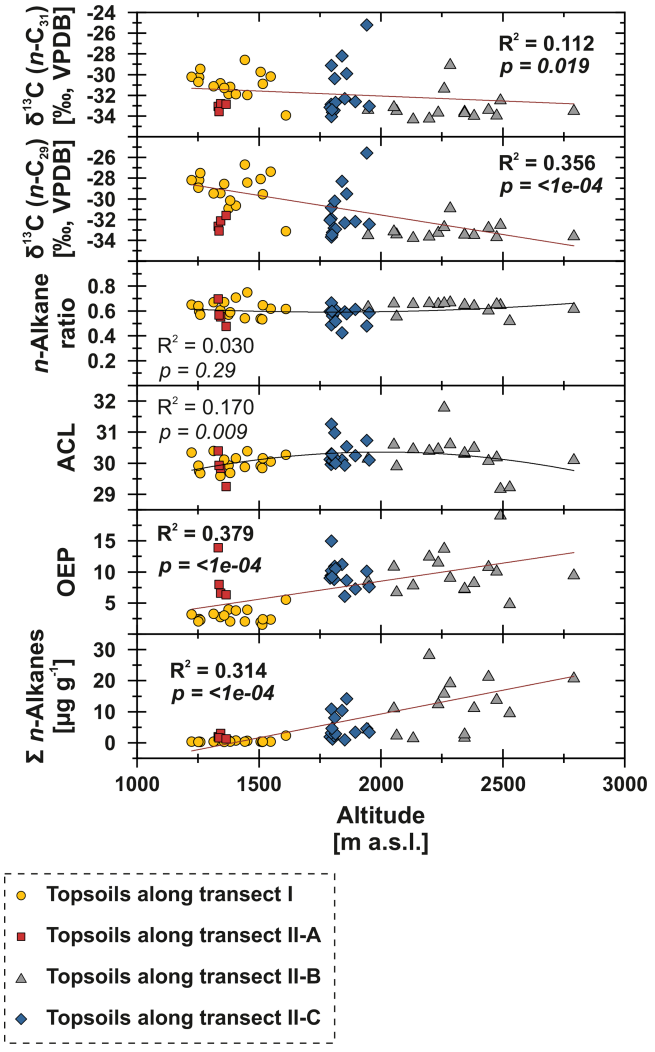

Figure 7. n-Alkane concentration (n-C_{25} – n-C_{35}), OEP, ACL, n-alkane ratio (n-C_{31} / (n-C_{29} + n-C_{31})) and compound-specific δ^{13}C (n-C_{29} and n-C_{31}) from Mongolian topsoils plotted against altitude (m a.s.l.; Jarvis et al., 2008). Red trend lines illustrate linear regressions, and black lines illustrate polynomial regressions. Bold values indicate significance ($\alpha = 0.05$).

only exceptions are the extreme values near Telmen Nuur, which are mostly due to the input of the ^{13}C-enriched succulent *Orostachys malacophylla*. As already proposed by Diefendorf et al. (2010), MAP is an intense predictor of δ^{13}C (n-C_{29}: $R^2 = 0.683$, $p =< 1e-04$; n-C_{31} : $R^2 = 0.343$, $p =< 1e-04$), which is further expressed in distinct linear correlations with the AI (Fig. 6). However, δ^{13}C also correlates with altitude; i.e. leaf wax ^{13}C shows a significant depletion with increasing altitude. Previous studies have shown strong positive correlations between δ^{13}C and altitude, indicating enhanced ^{13}C enrichment due to an altitude effect (Feakins et al., 2018) and/or environmental and climatic plant physiological adaptions, like a decrease in stomatal conductance with increasing altitude (Hultine and Marshall, 2000, and references therein). However, our data show the opposite behaviour, indicating that the observed ^{13}C enrichment is based on stomata conductance induced by climate (water stress) and not by altitude (Figs. 6, 7). Thus, the ^{13}C enrichment basically indicates the photorespiration of C_3 plants, affected by water availability and evapotranspiration and, thus, the WUE (Tipple and Pagani, 2007; Diefendorf and Freimuth, 2017).

5 Conclusions

This study investigates leaf wax n-alkane patterns and compound-specific δ^{13}C of modern plants and topsoils from semi-arid and arid Mongolia to test their chemotaxonomic potential and dependency on climate. Our results provide the first regional calibration of leaf wax n-alkanes for semi-arid and arid Mongolia, with the following results.

i. *Caragana* spp., *Artemisia* spp. and grasses (*Poaceae* and *Cyperaceae*) from semi-arid and arid Mongolia show distinct differences in their relative n-alkane patterns. n-Alkanes from the grasses are clearly dominated by n-C_{31}, whereas the woody shrub *Caragana* spp. is dominated by n-C_{29}. Since *Artemisia* species can grow both as herbaceous and woody shrubs, *Artemisia* spp. does not show a typical n-C_{31} dominance but is rather more equal to *Caragana* spp., with a dominance in n-C_{29}. *Larix* sp. is dominated by the mid-chain n-alkanes n-C_{23} and n-C_{25}. However, *Larix* sp. produces only few amounts of n-alkanes, and its dominance of mid-chain n-alkanes is not distinct in the respective topsoils. Thus, n-alkanes are not useful for reconstructing changes in the abundance of *Larix* sp. Although the ACL reveals no potential to discriminate between plant species, the most abundant n-alkanes, n-C_{29} and n-C_{31}, allow for discriminating between woody shrubs and grasses, which is expressed in the n-alkane ratio n-C_{31}/n-$C_{29} + n$-C_{31}.

ii. From plants to topsoils of transect II, the decrease in n-alkane concentrations and OEP values indicates n-alkane dilution with mineral soil components and ongoing n-alkane degradation. The n-alkane pattern of the topsoils is mainly characterised by a dominance of n-C_{31}, indicating dominant input from grasses. *Caragana*-covered sites tend to reflect the homologue pattern of *Caragana* spp., with n-C_{29} being the most dominant n-alkane. Topsoils under *Larix* sp. are dominated by the input from the grassy undergrowth. There are no significant differences in compound-specific δ^{13}C between plant species and topsoils. Topsoils tend to be 2 ‰ more enriched compared to the plants, indicating diagenesis from litter to topsoil.

iii. n-Alkane concentrations and OEP values from Mongolian topsoils are significantly correlated to climatic

parameters and decrease with increasing MAT and decreasing MAP. In contrast, our data indicate that the n-alkane patterns from the topsoils (ACL, n-alkane ratio) are not influenced by climatic parameters, and, thus, the n-alkane ratio can reliably be used to detect and reconstruct differences between the vegetation forms of grasses and woody shrubs. Although increasing altitude correlates with increasing n-alkane concentrations and OEP, altitude has no influences on the ACL and n-alkane ratio. For compound-specific δ^{13}C of the topsoils, strong correlations exist with increasing MAT and decreasing MAP, indicating an enhanced enrichment in ^{13}C with increasing aridity and drought stress. Although, δ^{13}C and altitude are also significantly negative correlated, the influence of altitude is negligible, since MAT decreases and MAP increases with altitude. Thus, leaf wax δ^{13}C is a valuable proxy for changes in climate and water use efficiency in semi-arid and arid Mongolia.

Our results show that the n-alkane homologues n-C_{29} and n-C_{31} have the chemotaxonomic power to differentiate between grasses and the woody shrub *Caragana* spp. Future studies on plant n-alkane patterns should include a detailed identification of plants regarding different species of each plant genus to reveal the full power of the n-alkane ratio as a vegetation proxy. This is particularly the case for different *Artemisia* species, which can so far not be separated from grasses and woody shrubs. While the n-alkane patterns are not biased by climatic influences, compound-specific δ^{13}C indicates a strong climatic dependency. Thus, n-alkanes and their compound-specific δ^{13}C can be potentially used as valuable proxies for future paleoenvironmental reconstruction based on leaf wax n-alkanes in sediment archives from semi-arid and arid Mongolia.

Data availability. Climate reanalysis data used in this study are based on the WorldClim 2 dataset of Fick and Hijmans (2017) and the Global Aridity Index and Potential Evapotranspiration (ET0) Climate Database v2 of Trabucco and Zomer (2019), which can be found online at http://worldclim.org/version2 (last access: 30 January 2020) and https://cgiarcsi.community/data/global-aridity-and-pet-database/ (last access: 30 January 2020), respectively.

The dataset that is used in this study is available in the Supplement.

Supplement. The supplement related to this article is available online at: https://doi.org/10.5194/bg-17-567-2020-supplement.

Author contributions. JuS, MB and RZ designed the study. MB and RZ collected samples along transect I in 2016. JuS and RZ collected samples along transect II in 2017. JuS carried out the major part of the laboratory analyses and was assisted by PS and MB. JeS conducted the statistical analyses. EB organised the plant determination and sample logistics. JuS, MB, PS and RZ wrote the paper, with contributions from JeS and EB.

Competing interests. The authors declare that they have no conflict of interest.

Acknowledgements. We thank the Swiss National Science Foundation (SNF) for funding (SNF: 150590). Furthermore we acknowledge our logistic partners in Mongolia and all field trip participants (2017 and 2018). For assistance in the laboratory, we would like to thank Magdalena Wagner and Felix Freitag, as well as Michael Zech, for scientific discussion.

Financial support. This research has been supported by the SNF (grant no. PP00P2-150590).

Review statement. This paper was edited by Frank Hagedorn and reviewed by two anonymous referees.

References

Aichner, B., Herzschuh, U., and Wilkes, H.: Influence of aquatic macrophytes on the stable carbon isotopic signatures of sedimentary organic matter in lakes on the Tibetan Plateau, Org. Geochem., 41, 706–718, https://doi.org/10.1016/j.orggeochem.2010.02.002, 2010a.

Aichner, B., Wilkes, H., Herzschuh, U., Mischke, S., and Zhang, C.: Biomarker and compound-specific δ^{13}C evidence for changing environmental conditions and carbon limitation at Lake Koucha, eastern Tibetan Plateau, J. Paleolimnology, 43, 873–899, https://doi.org/10.1007/s10933-009-9375-y, 2010b.

Aichner, B., Feakins, S. J., Lee, J. E., Herzschuh, U., and Liu, X.: High-resolution leaf wax carbon and hydrogen isotopic record of the late Holocene paleoclimate in arid Central Asia, Clim. Past, 11, 619–633, https://doi.org/10.5194/cp-11-619-2015, 2015.

Aichner, B., Hilt, S., Périllon, C., Gillefalk, M., and Sachse, D.: Biosynthetic hydrogen isotopic fractionation factors during lipid synthesis in submerged aquatic macrophytes: Effect of groundwater discharge and salinity, Org. Geochem., 113, 10–16, https://doi.org/10.1016/j.orggeochem.2017.07.021, 2017.

Aitchison, J.: The statistical analysis of compositional data, Blackburn Press, Caldwell, 460 pp., 2003.

Angst, G., John, S., Mueller, C. W., Kögel-Knabner, I., and Rethemeyer, J.: Tracing the sources and spatial distribution of organic carbon in subsoils using a multi-biomarker approach, Sci. Rep., 6, 29478, https://doi.org/10.1038/srep29478, 2016.

Bliedtner, M., Schäfer, I. K., Zech, R., and von Suchodoletz, H.: Leaf wax n-alkanes in modern plants and topsoils from eastern Georgia (Caucasus) – implications for reconstructing regional paleovegetation, Biogeosciences, 15, 3927–3936, https://doi.org/10.5194/bg-15-3927-2018, 2018a.

Bliedtner, M., Zech, R., Kühn, P., Schneider, B., Zielhofer, C., and von Suchodoletz, H.: The potential of leaf wax

biomarkers from fluvial soil-sediment sequences for paleovegetation reconstructions – Upper Alazani River, central southern Greater Caucasus (Georgia), Quaternary Sci. Rev., 196, 62–79, https://doi.org/10.1016/j.quascirev.2018.07.029, 2018b.

Boogaart, K. G. v. d.: Analyzing compositional data with R, Springer, Berlin, Heidelberg, 258 pp., 2013.

Boom, A., Carr, A. S., Chase, B. M., Grimes, H. L., and Meadows, M. E.: Leaf wax n-alkanes and δ^{13}C values of CAM plants from arid southwest Africa, Org. Geochem., 67, 99–102, https://doi.org/10.1016/j.orggeochem.2013.12.005, 2014.

Brittingham, A., Hren, M. T., and Hartman, G.: Microbial alteration of the hydrogen and carbon isotopic composition of n-alkanes in sediments, Org. Geochem., 107, 1–8, https://doi.org/10.1016/j.orggeochem.2017.01.010, 2017.

Buggle, B., Wiesenberg, G. L., and Glaser, B.: Is there a possibility to correct fossil n-alkane data for postsedimentary alteration effects?, Appl. Geochem., 25, 947–957, https://doi.org/10.1016/j.apgeochem.2010.04.003, 2010.

Bush, R. T. and McInerney, F. A.: Leaf wax n-alkane distributions in and across modern plants: Implications for paleoecology and chemotaxonomy, Geochim. Cosmochim. Ac., 117, 161–179, https://doi.org/10.1016/j.gca.2013.04.016, 2013.

Carr, A. S., Boom, A., Grimes, H. L., Chase, B. M., Meadows, M. E., and Harris, A.: Leaf wax n-alkane distributions in arid zone South African flora: Environmental controls, chemotaxonomy and palaeoecological implications, Org. Geochem., 67, 72–84, https://doi.org/10.1016/j.orggeochem.2013.12.004, 2014.

Castañeda, I. S., Mulitza, S., Schefuss, E., Lopes dos Santos, Raquel A., Sinninghe Damste, J. S., and Schouten, S.: Wet phases in the Sahara/Sahel region and human migration patterns in North Africa, P. Natl. Acad. Sci. USA, 106, 20159–20163, https://doi.org/10.1073/pnas.0905771106, 2009.

Cheung, M.-C., Zong, Y., Wang, N., Aitchison, J. C., and Zheng, Z.: δ^{13}C org and n-alkane evidence for changing wetland conditions during a stable mid-late Holocene climate in the central Tibetan Plateau, Palaeogeogr. Palaeocl., 438, 203–212, https://doi.org/10.1016/j.palaeo.2015.08.007, 2015.

Dashkhuu, D., Kim, J. P., Chun, J. A., and Lee, W.-S.: Long-term trends in daily temperature extremes over Mongolia, Weather and Climate Extremes, 8, 26–33, https://doi.org/10.1016/j.wace.2014.11.003, 2015.

Diefendorf, A. F. and Freimuth, E. J.: Extracting the most from terrestrial plant-derived n-alkyl lipids and their carbon isotopes from the sedimentary record: A review, Org. Geochem., 103, 1–21, https://doi.org/10.1016/j.orggeochem.2016.10.016, 2017.

Diefendorf, A. F., Mueller, K. E., Wing, S. L., Koch, P. L., and Freeman, K. H.: Global patterns in leaf δ^{13}C discrimination and implications for studies of past and future climate, P. Natl. Acad. Sci. USA, 107, 5738–5743, https://doi.org/10.1073/pnas.0910513107, 2010.

Diefendorf, A. F., Freeman, K. H., Wing, S. L., and Graham, H. V.: Production of n-alkyl lipids in living plants and implications for the geologic past, Geochim. Cosmochim. Ac., 75, 7472–7485, https://doi.org/10.1016/j.gca.2011.09.028, 2011.

Diefendorf, A. F., Leslie, A. B., and Wing, S. L.: Leaf wax composition and carbon isotopes vary among major conifer groups, Geochim. Cosmochim. Ac., 170, 145–156, https://doi.org/10.1016/j.gca.2015.08.018, 2015.

Eglinton, G. and Hamilton, R. J.: Leaf epicuticular waxes, Science (New York, NY), 156, 1322–1335, 1967.

Eglinton, T. I. and Eglinton, G.: Molecular proxies for paleoclimatology, Earth Planet. Sc. Lett., 275, 1–16, https://doi.org/10.1016/j.epsl.2008.07.012, 2008.

Farquhar, G. D., O'Leary, M. H., and Berry, J. A.: On the Relationship Between Carbon Isotope Discrimination and the Intercellular Carbon Dioxide Concentration in Leaves, Aust. J. Plant Physiol., 9, 121–137, https://doi.org/10.1071/PP9820121, 1982.

Feakins, S. J., Peters, T., Wu, M. S., Shenkin, A., Salinas, N., Girardin, C. A., Bentley, L. P., Blonder, B., Enquist, B. J., Martin, R. E., Asner, G. P., and Malhi, Y.: Production of leaf wax n-alkanes across a tropical forest elevation transect, Org. Geochem., 100, 89–100, https://doi.org/10.1016/j.orggeochem.2016.07.004, 2016.

Feakins, S. J., Wu, M. S., Ponton, C., Galy, V., and West, A. J.: Dual isotope evidence for sedimentary integration of plant wax biomarkers across an Andes-Amazon elevation transect, Geochim. Cosmochim. Ac., 242, 64–81, https://doi.org/10.1016/j.gca.2018.09.007, 2018.

Fick, S. E. and Hijmans, R. J.: WorldClim 2: New 1-km spatial resolution climate surfaces for global land areas, Int. J. Climatol., 37, 4302–4315, https://doi.org/10.1002/joc.5086, 2017.

Gao, L., Guimond, J., Thomas, E., and Huang, Y.: Major trends in leaf wax abundance, δ^{2}H and δ^{13}C values along leaf venation in five species of C_3 plants: Physiological and geochemical implications, Org. Geochem., 78, 144–152, https://doi.org/10.1016/j.orggeochem.2014.11.005, 2015.

Häggi, C., Eglinton, T. I., Zech, W., Sosin, P., and Zech, R.: A 250 ka leaf-wax δD record from a loess section in Darai Kalon, Southern Tajikistan, Quaternary Sci. Rev., 208, 118–128, https://doi.org/10.1016/j.quascirev.2019.01.019, 2019.

Harris, I., Jones, P. D., Osborn, T. J., and Lister, D. H.: Updated high-resolution grids of monthly climatic observations – the CRU TS3.10 Dataset, Int. J. Climatol., 34, 623–642, https://doi.org/10.1002/joc.3711, 2014.

Hilbig, W.: The vegetation of Mongolia, SPB Acad. Publ, Amsterdam, 258 pp., 1995.

Hoefs, M. J., Rijpstra, W. C., and Sinninghe Damsté, J. S.: The influence of oxic degradation on the sedimentary biomarker record I: Evidence from Madeira Abyssal Plain turbidites, Geochim. Cosmochim. Ac., 66, 2719–2735, https://doi.org/10.1016/S0016-7037(02)00864-5, 2002.

Hoffmann, B., Kahmen, A., Cernusak, L. A., Arndt, S. K., and Sachse, D.: Abundance and distribution of leaf wax n-alkanes in leaves of Acacia and Eucalyptus trees along a strong humidity gradient in northern Australia, Org. Geochem., 62, 62–67, https://doi.org/10.1016/j.orggeochem.2013.07.003, 2013.

Howard, S., McInerney, F. A., Caddy-Retalic, S., Hall, P. A., and Andrae, J. W.: Modelling leaf wax n-alkane inputs to soils along a latitudinal transect across Australia, Org. Geochem., 121, 126–137, https://doi.org/10.1016/j.orggeochem.2018.03.013, 2018.

Hultine, K. R. and Marshall, J. D.: Altitude trends in conifer leaf morphology and stable carbon isotope composition, Oecologia, 123, 32–40, https://doi.org/10.1007/s004420050986, 2000.

Jarvis, A., Reuter, H. I., Nelson, A., and Guevara, E.: Hole-filled seamless SRTM data V4, International Centre for Tropical Agriculture (CIAT), http://srtm.csi.cgiar.org (last access: 30 January 2020), 2008.

Klinge, M. and Sauer, D.: Spatial pattern of Late Glacial and Holocene climatic and environmental development in Western Mongolia – A critical review and synthesis, Quaternary Sci. Rev., 210, 26–50, https://doi.org/10.1016/j.quascirev.2019.02.020, 2019.

Klinge, M., Lehmkuhl, F., Schulte, P., Hülle, D., and Nottebaum, V.: Implications of (reworked) aeolian sediments and paleosols for Holocene environmental change in Western Mongolia, Geomorphology, 292, 59–71, https://doi.org/10.1016/j.geomorph.2017.04.027, 2017.

Kölbl, A., Steffens, M., Wiesmeier, M., Hoffmann, C., Funk, R., Krümmelbein, J., Reszkowska, A., Zhao, Y., Peth, S., Horn, R., Giese, M., and Kögel-Knabner, I.: Grazing changes topography-controlled topsoil properties and their interaction on different spatial scales in a semi-arid grassland of Inner Mongolia, P. R. China, Plant Soil, 340, 35–58, https://doi.org/10.1007/s11104-010-0473-4, 2011.

Lane, C. S.: Modern n-alkane abundances and isotopic composition of vegetation in a gymnosperm-dominated ecosystem of the southeastern US coastal plain, Org. Geochem., 105, 33–36, https://doi.org/10.1016/j.orggeochem.2016.12.003, 2017.

Li, G., Li, L., Tarozo, R., Longo, W. M., Wang, K. J., Dong, H., and Huang, Y.: Microbial production of long-chain n-alkanes: Implication for interpreting sedimentary leaf wax signals, Org. Geochem., 115, 24–31, https://doi.org/10.1016/j.orggeochem.2017.10.005, 2018a.

Li, X., Anderson, B. J., Vogeler, I., and Schwendenmann, L.: Long-chain n-alkane and n-fatty acid characteristics in plants and soil – potential to separate plant growth forms, primary and secondary grasslands?, Sci. Total Environ., 645, 1567–1578, https://doi.org/10.1016/j.scitotenv.2018.07.105, 2018b.

Liu, J., An, Z., and Liu, H.: Leaf wax n-alkane distributions across plant types in the central Chinese Loess Plateau, Org. Geochem., 125, 260–269, https://doi.org/10.1016/j.orggeochem.2018.09.006, 2018.

Peck, J. A., Khosbayar, P., Fowell, S. J., Pearce, R. B., Ariunbileg, S., Hansen, B. C., and Soninkhishig, N.: Mid to Late Holocene climate change in north central Mongolia as recorded in the sediments of Lake Telmen, Palaeogeogr. Palaeocl., 183, 135–153, https://doi.org/10.1016/S0031-0182(01)00465-5, 2002.

Poynter, J. G., Farrimond, P., Robinson, N., and Eglinton, G.: Aeolian-Derived Higher Plant Lipids in the Marine Sedimentary Record: Links with Palaeoclimate, in: Paleoclimatology and Paleometeorology: Modern and Past Patterns of Global Atmospheric Transport, edited by: Leinen, M. and Sarnthein, M., NATO ASI Series, Series C, Springer, Dordrecht, 282, 435–462, https://doi.org/10.1007/978-94-009-0995-3, 1989.

Prokopenko, A. A., Khursevich, G. K., Bezrukova, E. V., Kuzmin, M. I., Boes, X., Williams, D. F., Fedenya, S. A., Kulagina, N. V., Letunova, P. P., and Abzaeva, A. A.: Paleoenvironmental proxy records from Lake Hovsgol, Mongolia, and a synthesis of Holocene climate change in the Lake Baikal watershed, Quaternary Res., 68, 2–17, https://doi.org/10.1016/j.yqres.2007.03.008, 2007.

Pyankov, V. I., Gunin, P. D., Tsoog, S., and Black, C. C.: C_4 plants in the vegetation of Mongolia: Their natural occurrence and geographical distribution in relation to climate, Oecologia, 123, 15–31, https://doi.org/10.1007/s004420050985, 2000.

R Core Team: R: A Language and Environment for Statistical Computing, https://www.R-project.org/ (last access: 30 January 2020), 2019.

Rach, O., Engels, S., Kahmen, A., Brauer, A., Martín-Puertas, C., van Geel, B., and Sachse, D.: Hydrological and ecological changes in western Europe between 3200 and 2000 years BP derived from lipid biomarker δD values in lake Meerfelder Maar sediments, Quaternary Sci. Rev., 172, 44–54, https://doi.org/10.1016/j.quascirev.2017.07.019, 2017.

Rao, M. P., Davi, N. K., D'Arrigo, R. D., Skees, J., Nachin, B., Leland, C., Lyon, B., Wang, S.-Y., and Byambasuren, O.: Dzuds, droughts, and livestock mortality in Mongolia, Environ. Res. Lett., 10, 074012, https://doi.org/10.1088/1748-9326/10/7/074012, 2015.

Rao, Z., Jia, G., Li, Y., Chen, J., Xu, Q., and Chen, F.: Asynchronous evolution of the isotopic composition and amount of precipitation in north China during the Holocene revealed by a record of compound-specific carbon and hydrogen isotopes of long-chain n-alkanes from an alpine lake, Earth Planet. Sc. Lett., 446, 68–76, https://doi.org/10.1016/j.epsl.2016.04.027, 2016.

Rao, Z., Guo, W., Cao, J., Shi, F., Jiang, H., and Li, C.: Relationship between the stable carbon isotopic composition of modern plants and surface soils and climate: A global review, Earth-Sci. Rev., 165, 110–119, https://doi.org/10.1016/j.earscirev.2016.12.007, 2017.

Rommerskirchen, F., Eglinton, G., Dupont, L., and Rullkötter, J.: Glacial/interglacial changes in southern Africa: Compound-specific $\delta^{13}C$ land plant biomarker and pollen records from southeast Atlantic continental margin sediments, Geochem. Geophy. Geosy., 7, 1–21, https://doi.org/10.1029/2005GC001223, 2006.

Rudaya, N. and Li, H.-C.: A new approach for reconstruction of the Holocene climate in the Mongolian Altai: The high-resolution $\delta^{13}C$ records of TOC and pollen complexes in Hoton-Nur Lake sediments, J. Asian Earth Sci., 69, 185–195, https://doi.org/10.1016/j.jseaes.2012.12.002, 2013.

Sachse, D., Radke, J., and Gleixner, G.: δD values of individual n-alkanes from terrestrial plants along a climatic gradient – Implications for the sedimentary biomarker record, Org. Geochem., 37, 469–483, https://doi.org/10.1016/j.orggeochem.2005.12.003, 2006.

Schäfer, I. K., Lanny, V., Franke, J., Eglinton, T. I., Zech, M., Vysloužilová, B., and Zech, R.: Leaf waxes in litter and topsoils along a European transect, SOIL, 2, 551–564, https://doi.org/10.5194/soil-2-551-2016, 2016.

Schäfer, I. K., Bliedtner, M., Wolf, D., Kolb, T., Zech, J., Faust, D., and Zech, R.: A $\delta^{13}C$ and $\delta^{2}H$ leaf wax record from the Late Quaternary loess-paleosoil sequence El Paraíso, Central Spain, Palaeogeogr. Palaeocl., 507, 52–59, https://doi.org/10.1016/j.palaeo.2018.06.039, 2018.

Schefuss, E., Schouten, S., and Schneider, R. R.: Climatic controls on central African hydrology during the past 20,000 years, Nature, 437, 1003–1006, https://doi.org/10.1038/nature03945, 2005.

Schulz, S., Giebler, J., Chatzinotas, A., Wick, L. Y., Fetzer, I., Welzl, G., Harms, H., and Schloter, M.: Plant litter and soil type drive abundance, activity and community structure of alkB harbouring microbes in different soil compartments, ISME J., 6, 1763–1774, https://doi.org/10.1038/ismej.2012.17, 2012.

Schwark, L., Zink, K., and Lechterbeck, J.: Reconstruction of postglacial to early Holocene vegetation history in terrestrial Central Europe via cuticular lipid biomarkers and pollen records from lake sediments, Geology, 30, 463–466, https://doi.org/10.1130/0091-7613(2002)030<0463:ROPTEH>2.0.CO;2, 2002.

Shepherd, T. and Wynne Griffiths, D.: The effects of stress on plant cuticular waxes, New Phytol., 171, 469–499, https://doi.org/10.1111/j.1469-8137.2006.01826.x, 2006.

Su, P., Xie, T., and Zhou, Z.: C_4 plant species and geographical distribution in relation to climate in the desert vegetation of China, Sciences in Cold and Arid Regions, 3, 381–391, 2011.

Sun, Q., Xie, M., Lin, Y., Shan, Y., Zhu, Q., Xu, D., Su, Y., Rioual, P., and Chu, G.: An n-alkane and carbon isotope record during the last deglaciation from annually laminated sediment in Lake Xiaolongwan, northeastern China, J. Paleolimnol., 56, 189–203, https://doi.org/10.1007/s10933-016-9904-4, 2016.

Tipple, B. J. and Pagani, M.: The Early Origins of Terrestrial C_4 Photosynthesis, Annu. Rev. Earth Pl. Sc., 35, 435–461, https://doi.org/10.1146/annurev.earth.35.031306.140150, 2007.

Tipple, B. J., Berke, M. A., Doman, C. E., Khachaturyan, S., and Ehleringer, J. R.: Leaf-wax n-alkanes record the plant-water environment at leaf flush, P. Natl. Acad. Sci. USA, 110, 2659–2664, https://doi.org/10.1073/pnas.1213875110, 2013.

Trabucco, A. and Zomer, R.: Global Aridity Index and Potential Evapotranspiration (ET0) Climate Database v2, https://doi.org/10.6084/M9.FIGSHARE.7504448.V3, 2019.

Vogts, A., Moossen, H., Rommerskirchen, F., and Rullkötter, J.: Distribution patterns and stable carbon isotopic composition of alkanes and alkan-1-ols from plant waxes of African rain forest and savanna C_3 species, Org. Geochem., 40, 1037–1054, https://doi.org/10.1016/j.orggeochem.2009.07.011, 2009.

Wang, J., Axia, E., Xu, Y., Wang, G., Zhou, L., Jia, Y., Chen, Z., and Li, J.: Temperature effect on abundance and distribution of leaf wax n-alkanes across a temperature gradient along the 400 mm isohyet in China, Org. Geochem., 120, 31–41, https://doi.org/10.1016/j.orggeochem.2018.03.009, 2018a.

Wang, J., Xu, Y., Zhou, L., Shi, M., Axia, E., Jia, Y., Chen, Z., Li, J., and Wang, G.: Disentangling temperature effects on leaf wax n-alkane traits and carbon isotopic composition from phylogeny and precipitation, Org. Geochem., 126, 13–22, https://doi.org/10.1016/j.orggeochem.2018.10.008, 2018b.

Wang, W. and Feng, Z.: Holocene moisture evolution across the Mongolian Plateau and its surrounding areas: A synthesis of climatic records, Earth-Sci. Rev., 122, 38–57, https://doi.org/10.1016/j.earscirev.2013.03.005, 2013.

Wang, W., Ma, Y., Feng, Z., Narantsetseg, T., Liu, K.-B., and Zhai, X.: A prolonged dry mid-Holocene climate revealed by pollen and diatom records from Lake Ugii Nuur in central Mongolia, Quaternary Int., 229, 74–83, https://doi.org/10.1016/j.quaint.2010.06.005, 2011.

Wang, Z., Liu, H., and Cao, Y.: Choosing a suitable ε_{w-p} spatial distribution in China, Org. Geochem., 121, 161–168, https://doi.org/10.1016/j.orggeochem.2018.01.002, 2018.

Wu, M. S., West, A. J., and Feakins, S. J.: Tropical soil profiles reveal the fate of plant wax biomarkers during soil storage, Org. Geochem., 128, 1–15, https://doi.org/10.1016/j.orggeochem.2018.12.011, 2019.

Zech, M., Buggle, B., Leiber, K., Marković, S., Glaser, B., Hambach, U., Huwe, B., Stevens, T., Sümegi, P., Wiesenberg, G., and Zöller, L.: Reconstructing Quaternary vegetation history in the Carpathian Basin, SE-Europe, using n-alkane biomarkers as molecular fossils, E&G – Quaternary Sci. J., 58, 148–155, https://doi.org/10.3285/eg.58.2.03, 2009.

Zech, M., Andreev, A., Zech, R., Mäller, S., Hambach, U., Frechen, M., and Zech, W.: Quaternary vegetation changes derived from a loess-like permafrost palaeosol sequence in northeast Siberia using alkane biomarker and pollen analyses, Boreas, 540–550, https://doi.org/10.1111/j.1502-3885.2009.00132.x, 2010.

Zech, R., Zech, M., Marković, S., Hambach, U., and Huang, Y.: Humid glacials, arid interglacials? Critical thoughts on pedogenesis and paleoclimate based on multi-proxy analyses of the loess–paleosol sequence Crvenka, Northern Serbia, Palaeogeogr. Palaeocl., 387, 165–175, https://doi.org/10.1016/j.palaeo.2013.07.023, 2013.